International Journal of Materials Engineering 2013, 3(6): 124-135
DOI: 10.5923/j.ijme.20130306.02

Nanosized TiO_2 - Based Mixed Oxide Films: Sol-gel Synthesis, Structure, Electrochemical Characteristics and Photocatalytic Activity

Nataliia Smirnova[1,*], Yuriy Gnatyuk[1], Nadiia Vityuk[1], Oksana Linnik[1], Anna Eremenko[1], Vera Vorobets[2], Gennadiy Kolbasov[2]

[1]Chuiko Institute of Surface Chemistry, Ukrainian National Academy of Sciences, 17 Gen. Naumov str., Kyiv, 03164, Ukraine
[2]Institute of General & Inorganic Chemistry, Ukrainian National Academy of Sciences, 32/34 Palladin str., Kyiv, 03680, Ukraine

Abstract A variety of mixed oxide nanostructured films (mesoporous TiO_2/ZnO and TiO_2/ZrO_2, nonporous $SiO_2/TiO_2/ZrO_2$) was synthesized by sol-gel method on the glass, titanium and silicon substrates using metal alkoxides (tetraethoxysilane, titanium tetraisopropoxide and zirconium tetrapropoxide) or (Zn $(Ac)_2$) as precursors and Pluronic P123 as a template agent for mesoporous structure formation. TiO_2 films alone and TiO_2/oxide composites were characterized using hexane adsorption, XRD, XPS, Raman and UV/vis spectroscopy. Band gap energy and the position of flatband potentials were estimated by photoelectrochemical measurements. On the base of analysis of the detail XPS spectra it was found the formation of Ti – O – Zn, Ti – O – Zr, Si – O – Ti, Si – O – Zr, Si – O – Ti – O – Zr bonds. Detected by XPS oxygen and silicon peak positions evolution correlated with E_g reduction of analyzed ternary mixed oxides and with the photocatalytic behavior of the films as well. An enhancement of photocatalytic activity of zirconia-doped films in comparison with that of pure TiO_2 originated from an anodic shift of the valence band edge potential. Catalytic activity of mesoporous TiO_2/ZnO and TiO_2/ZrO_2 films in the process of Cr^{VI} to Cr^{III} photoreduction was improved with increasing of surface acidity and specific surface area of the samples.

Keywords Nanosized TiO_2 – Based Mixed Oxide Films, Structure, Photocatalysis

1. Introduction

Widespread use of a semiconductor photocatalysts for environmentally important processes of neutralization of toxic organic compounds and heavy metals in the waste water, drinking water and air caused by the need to create new nanomaterials based on titanium dioxide with high surface area, define structure, extended to the visible spectral range. It is known that TiO_2 effectiveness could be improved by mixing with other oxides that control structure-sorption, optical and electronic properties[1-5]. Coupling of two semiconductors[6, 7] is useful to achieve a more efficient separation of photogenerated electron-hole pair that led to improvement of the photoactivity. Also, it is found that the photocatalytic activity depends on the phase composition and crystalline size that modify the TiO_2 band gap[8-10]. The size effect on the phase stability of nanostructures manifested in the stabilization of new phases, which is not characteristic to a bulk crystal, in some cases – amorphous[11]. Authors[12, 13] found out that the transformation sequence and thermodynamic phase stability depended on the initial particle sizes. For instance, rutile is most stable crystalline phase of TiO_2 in bulk, when anatase is thermodynamically stable in nanosized materials.

Sol-gel technology is one of the most practically useful techniques to prepare nanostructured complex oxide mixtures with atomic level mixing of the components. Generalized method for the synthesis of transition-metal oxides with high surface areas using the block copolymers as structure-directing agents was reported by[14] and used for thin film of titanium dioxide formation[15]. In our previous work, this approach has been extended to produce mixed oxide nanocomposites. Recently, we studied sol-gel TiO_2 films doped with transition metal ions, zirconium and zinc oxides in respect to their structural, optical and photocatalytic properties[16-21]. Depending on the component ratios and conditions of thermal treatment the sol-gel method allows to obtain: 1) the products of replacement of the titanium ions in TiO_2 crystal lattice by transition metal ions[17]; 2) solid solutions ($Ti_{1-x}Zr_xO_2$)[18, 19] or 3) spinel phases – $ZnTiO_3$, $Zn_2Ti_3O_8$[20-22], Ti_2ZrO_6[23, 24] and $Fe_2Ti_2O_7$[25]. The aim of the present paper is to discuss the phase composition, electronic

* Corresponding author:
smirnat@i.ua (Nataliia Smirnova)
Published online at http://journal.sapub.org/ijme

structure, electrochemical characteristics and their effect on the photocatalytic activity of sol-gel obtained mixed oxide films based on TiO_2.

2. Experimental

2.1. Synthesis of Materials

All reagents (Aldrich, reagent grade) were used as received. Template sol-gel method was applied for preparation of mesoporous TiO_2/ZnO, TiO_2/ZrO_2 and nonporous $TiO_2/ZrO_2/SiO_2$ ternary films at glass, silicon and aluminum substrates. Such alkoxides as tetraethoxysilane (TEOS), titanium tetraisopropoxide (TTIP) and zirconium tetrapropoxide (ZTP) were mixed with a water-ethanol solution for pre-hydrolysis. 1 M HNO_3 solution was used to adjust pH value on hydrolysis of TEOS. Hydrolysis of TTIP and ZTP is very fast in the presence of water resulting in the formation of precipitated. To prevent fast precipitation of titanium and zirconium hydroxides acetylacetone (acac) as a complexing agent was added to the solution. Ethanol solution of a template agent (nonionic triblock-copolymer of propyleneoxide with ethyleneoxide $EO_{20}PO_{70}EO_{20}$, Pluronic P123) was added to the solution of alkoxides after their pre-hydrolysis for 4-16 h to form ordered mesopores in the films. For TiO_2/ZnO films preparation zinc acetate (Aldrich) was used as metal source. The molar ratios of the components were as follow $Ti(i\text{-}Pro)_4$: $Zn(CH_3COO)_2$: P123 : acetylacetone : H_2O : C_2H_5OH : HNO_3 as 1 : 0.01 : 0.05 : 0.5 : 1 : 40 : 1. The final molar ratio of components for the synthesis of TiO_2/ZrO_2 mesoporous films was $Ti(OPr)_4^i$: $Zr(OPr)_4^i$: P123 : acac : HNO_3 : H_2O : C_2H_5OH = 1 – 0.7 : 0 – 0.3 : 0.05 : 0.5 : 0.016 : 10 : 41. Precursor of nonporous ternary $TiO_2/ZrO_2/SiO_2$ film was prepared by addition of TTIP and ZTP (TiO_2:ZrO_2=0.7:0.3) acetylacetone solutions to prehydrolysed TEOS to adjust TiO_2:ZrO_2:SiO_2=21:9:70 or 49:21:30 composition.

For film deposition onto glass, silicon wafer or titanum substrates, dip-coating technique was utilized. After deposition of the film, gelation and gel ripening, it was dried in air at room temperature for 2 h (dried samples). Then the dried films were sintered in a furnace at a heating rate $\beta = 2$ K/min to 523 K, and at $\beta = 0.25$ K/min from 523 to 623 K. P123 burns out at these temperatures and this process should be carefully carried out for keeping the ordered porous structure of the oxide film. Then temperature was elevated to 773 at $\beta = 3$ K/min and the systems were kept at a certain temperature for 3 h.

To facilitate structural investigations by XRD and Raman spectroscopy powders with the same chemical composition have been prepared via gelation of the films' precursors, their drying in air with following heat treatment according to the scheme described for the films

2.2. Characterization Techniques

XRD analysis of crystalline phases was performed using a DRON-4-07 (Burevestnik, St. Petersburg) diffractometer (Cu K_α radiation with Ni filter) with Brag-Brentano registration geometry (2θ = 10–60°). The average size of crystallites was determined using Sherrer equation applied to the most intensive peak. The degree of the powders crystallinity was estimated as the ratio of integrated intensities, such as for the (101) line of the studied and reference standard samples (reference standard: TiO_2, anatase 100%).

The Raman spectra were detected by an automated double spectrometer DFS-24 (LOMO, Russia), followed by a cooled photomultiplier and registration system working in a photon counting mode. In connection to numerical analysis the spectra were digitalized in wide frequency range with a fixed increment (from 1 cm–1 up to 5 cm–1). For obtaining more reliable information, additional noise minimization technique was applied. In particular, relatively wide spectral windows of ~ 3-5 cm^{-1}, long acquisition time and optimized digital averaging of the spectra with a variable spectral window were used for weak signal amplification. The spectra were excited by radiation of Ar-ion laser (at λL=514.5 nm).

The electronic structure of the sol-gel film surface was explored by X-ray photoelectron spectroscopy (XPS) by electron spectrometer (E MgKα =1253.6 eV, $P = 10^{-7}$ Pa) with PHOIBOS-100 energy analyzer SPECS (USA). The XPS peak decomposition was carried out by Gauss–Newton method, the area of peaks was determined after subtraction of background by Shirley method.

The photoelectrochemical properties of the TiO_2/ZnO and TiO_2/ZrO_2 electrodes were estimated using the spectral dependence of the photoelectrochemical current ($i_{ph.}$), measured with a commercial spectrometer KSVU-1 (LOMO, Russia) with spectral resolution 1 nm. The experiments were carried out at 22°C under pure argon bubbling in the temperature-controlled quartz cell. The i_{ph} spectra were measured with usage of the mechanical light chopper of 20 Hz frequencies and standard circuit synchronous detection. A high-pressure xenon lamp with stabilized discharge current was used as light source. The i_{ph} spectra were expressed in units of quantum efficiency (electron/photon). The resistivity of TiO_2/ZrO_2 films on Ti substrate was measured by means of common alternating current bridge BM401. Ag/AgCl electrode was used as the reference electrode on the pH value of the electrolyte.

Photocatalytic activity of synthesized films has been checked in the process of Cr*(*VI*)* to Cr*(*III*)* photoreduction in water solution of $K_2Cr_2O_7$ ($C_M = 2\ 10^{-4}$M) in the presence of EDTA ($C_M = 2 \cdot 10^{-4}$ M) at pH = 2[26]. The open reactor with the reaction components (enabled continues inflow of oxygen) was irradiated with an UV light of mercury lamp PRK- 1000 with $P_0 = 3\ 10^{-7}$einstein $dm^{-3}\ s^{-1}$ intensity. Running water was circulated through the jacket to ensure constant temperature of the magnetically stirred reaction mixture. During the experiments concentration of reagents has been controlled with an UV-VIS spectrometer Perkin-Elmer Lambda-35. Half time of conversion Cr(VI) to Cr(III) in 20 ml of $2 \cdot 10^{-4}$ M water solution of $K_2Cr_2O_7$ in the

presence of EDTA ($2 \cdot 10^{-4}$ M) at pH=2 over 1 film (m=0.001g).

3. Results and Discussion

3.1. Phase Composition and Electronic Structure of TiO_2/ZnO Films

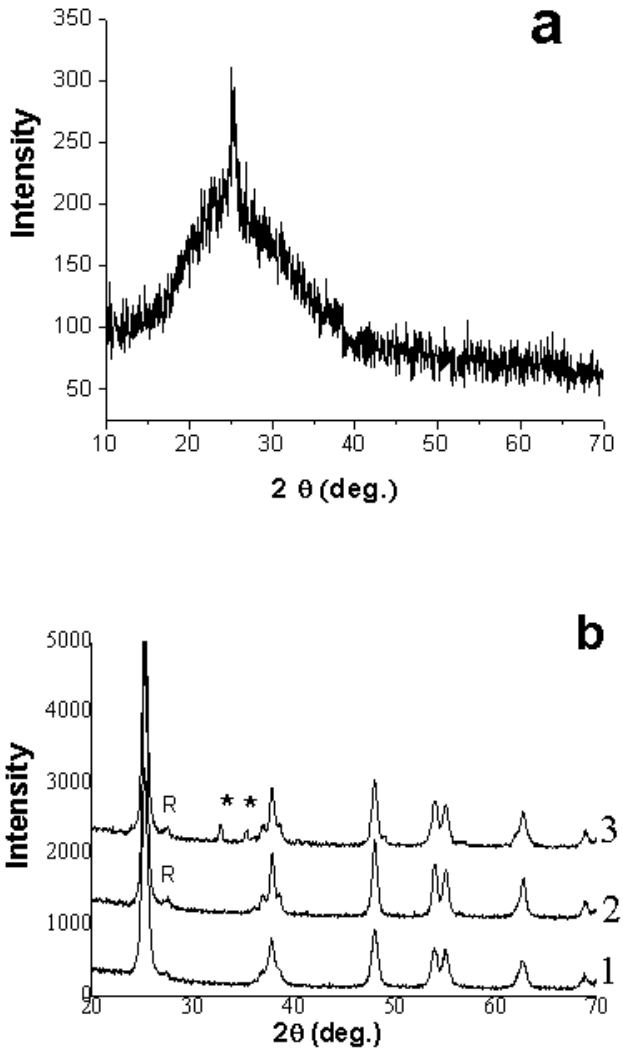

Figure 1. (a) X-Ray diffraction patterns of TiO_2/ZnO (1%) film; and (b) powders TiO_2 (1), TiO_2/5 atom % ZnO (2) and TiO_2/10 atom % ZnO (3) calcined at 773K. * lables peaks for the new phase $ZnTiO_3$, R - ruthile

The entire As we reported previously[21] hexane adsorption-desorption isotherms of the 500°C calcined TiO_2/ZnO films indicated mesoporosity[27] with hysteresis loop, which suggested bimodal porous size distribution with main pore sizes at r~ 4 and 8-10 nm. The specific surface area (S_{BET} ~ 300 m^2/g) was yielded from BET analysis of the isotherms for all TiO_2 and TiO_2/ZnO samples. Freshly prepared TiO_2 and TiO_2/ZnO films on glass showed highly hydrophilic properties, their water contact angles being ca. 5–7. Films with low Zn content (< 5%) differed significantly from pure TiO_2 films and showed super-hydrophilicity with a water contact angle near 0.

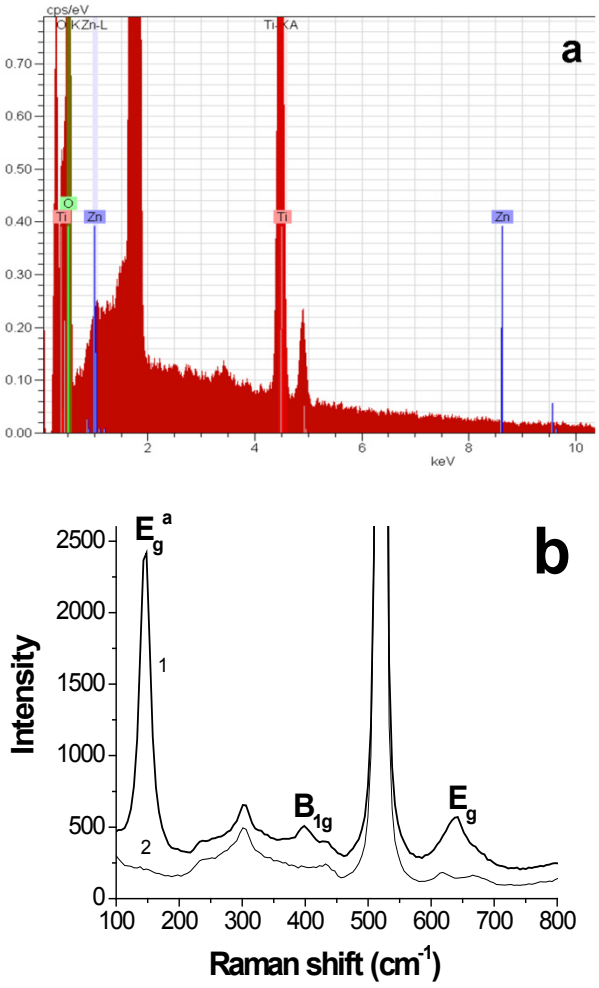

Figure 2. (a) X-ray analysed EDS spectra of Zn^{2+}/TiO_2 films and (b) Raman spectra of Zn^{2+}/TiO_2 film (1), and Si wafer (2)

The crystalline structures of TiO_2/ZnO nanocomposites with dopant contents in the range 1–10 atom % were studied by XRD measurements of powders prepared from the precursor (Figure 1). The XRD patterns of TiO_2 and TiO_2/1 atom % ZnO only exhibited diffraction lines which were attributable to the crystalline anatase phase. When the dopant content was increased (up to 5 atom % ZnO), a very weak diffraction line assigned to the crystalline rutile phase of TiO_2 was observed, while new peaks characteristic of the $ZnTiO_3$ perowskite phase appeared in the XRD pattern for the TiO_2/10 atom % ZnO sample. The initial crystallinity of the titania films (60%) slightly increased as the Zn content of the films increased. The average size of the anatase crystallites estimated via the Scherrer equation increased from 13 nm for TiO_2 to 15–17 nm for the TiO_2/ZnO powders.

EDS EDS analysis of Zn^{2+}/TiO_2 films using X-ray detector testified that zinc ions are present rather in the bulk (Fig. 2, a) than on the surface of film.

In terms of Raman spectroscopy, a well-resolved Raman peak at 145 cm^{-1} attributing to the main E_g anatase vibration mode and vibration peaks at 397 (B_{1g}) and 638 cm^{-1} (E_g) are detected in the spectrum of Zn^{2+}/TiO_2 film. It was

reported[28] that the Raman band shift towards higher wavenumber and their maximum widening coincide with the titania particle size decrease.

Chemical state of elements and relationship between the matrix structures on the surface of films are investigated by XPS[20]. Nonsymmetrical Ti (2p) peaks registered in the spectra of all samples were deconvoluted (Fig 3, a) as the sum of 458.9 and 458.5 eV peaks corresponded to Ti-O-Ti and Ti-O-Zn bonds. In the region of $Zn2p_{3/2}$ signal the peak (Fig. 3, b) attributed[29] to the formation of Ti-O-Zn (E_{BE}=1022.5 eV) and Zn-O-Zn bonds (E_{BE}=1021.7 eV) were registered.

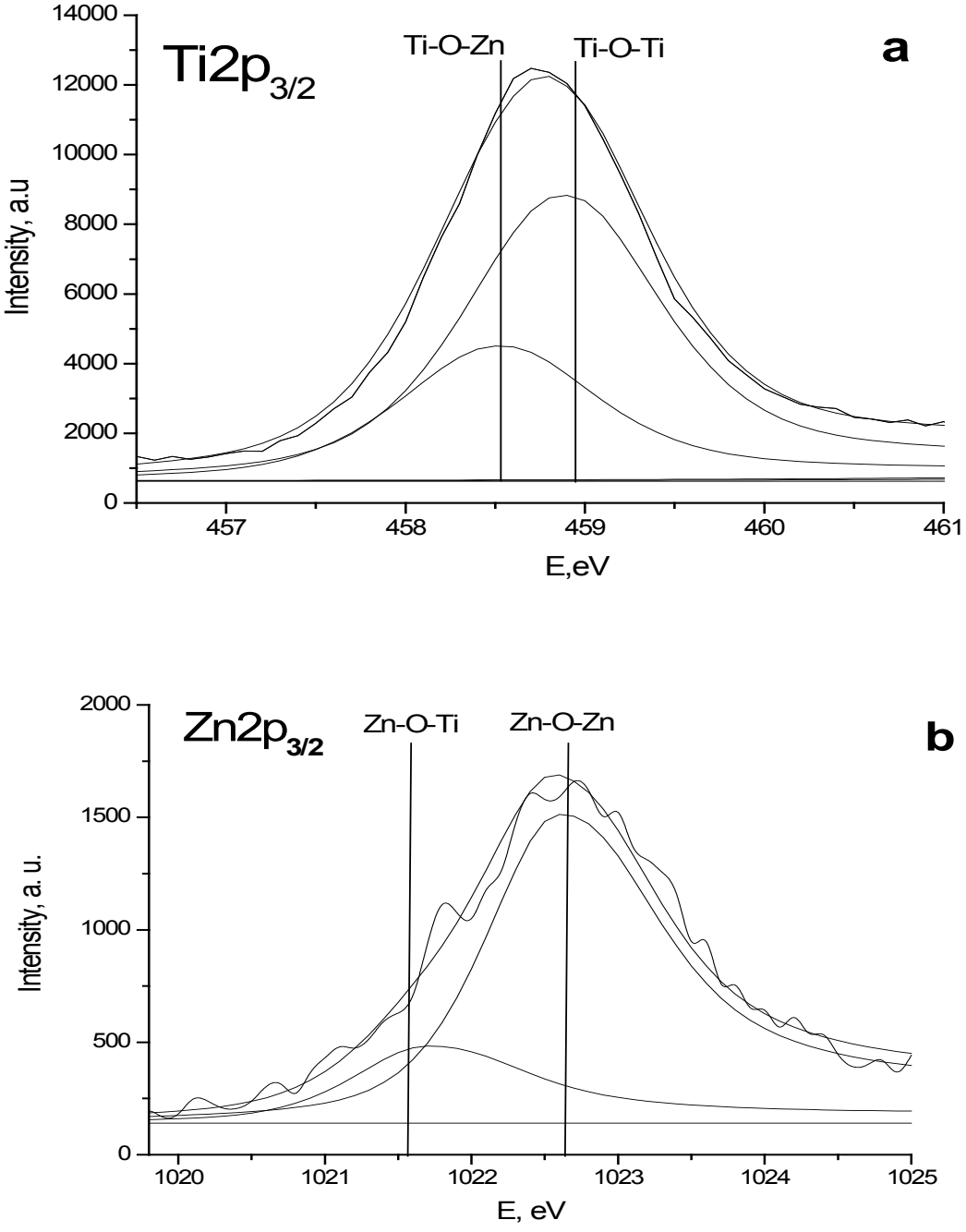

Figure 3. XPS spectra of Zn2p – a, and Ti2p - b levels for Zn^{2+}/TiO_2 deconvoluted into components

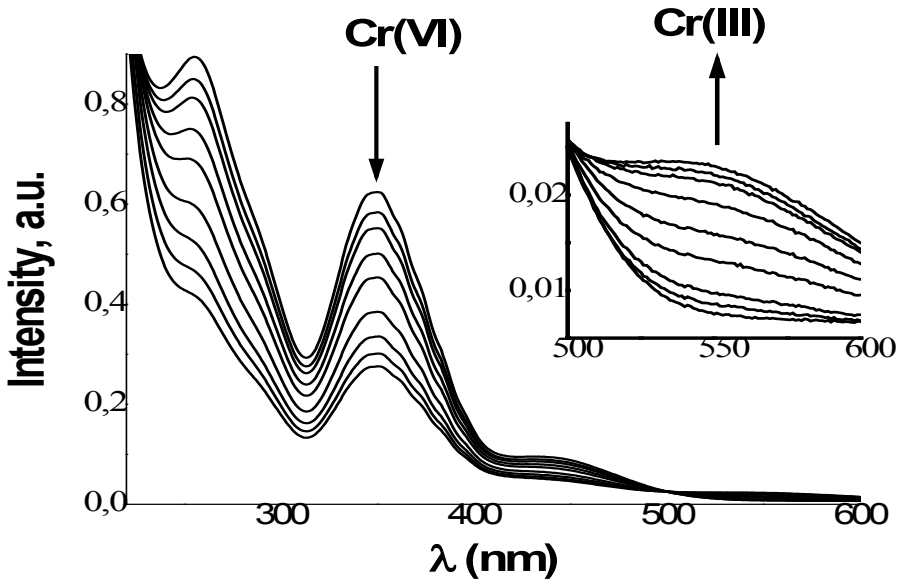

Figure 4. UV absorption spectra changes in Cr(VI) to Cr (III) photoreduction in presence of Na_2EDTA over 1%ZnO/TiO_2 film. Spectra were registered after 10, 20, 40, 60, 100, 140, 180 and 220 min under UV irradiation.[$K_2Cr_2O_7$] =[EDTA] = $2 \cdot 10^{-4}$ mol/l, pH = 2 ($HClO_4$)

The O*1s* spectra (not shown here) were separated into two main contributions that were assigned to the "O^{2-}" anions of the crystalline network (near 530.0 eV) and integrated as –OH (532.5 eV) and adsorbed H_2O (533.0 eV). The first peak is slightly shifted to lower E_B value for the TiO_2/ZnO due to Ti–O–Zn bonds formation. As we reported previously [21] the total surface acid site density (B-centres + L-centres) according to Tanabe model[30] increased with zinc content.

3.2. Photoelectrochemical Characteristics and Photocatalytic Properties of TiO_2/ZnO Films

The position of the flatband potential (U_{fb}) of titania and TiO_2/ZnO films coated on the titanium substrates were estimated from photocurrent (i_{ph}) plotted against applied potential by extrapolation straight line of these dependences to the abscissa[31]. The enhancement of photocurrent generation efficiency indicate that Zn^{2+} ions addition is beneficial to promote charge separation within nanostructured TiO_2 film and improve interfacial charge transfer process. Flatband potential values for the mesoporous TiO_2 and TiO_2/ZnO samples are listed in Table 1.

Table 1. The values of band gap (E_g,), flat-band potential (E_{fb} *vs* NHE) of TiO_2 and TiO_2/ZnO films and their photocatalytic efficiency in process of Cr (VI) to Cr(III) photoreduction

Sample	E_{fb} *vs* NHE	Photocatalytic efficiency k, sec^{-1}
TiO_2	-0.51	0.22×10^{-4}
TiO_2/ZnO (1%)	-1.21	0.30×10^{-4}
TiO_2/ZnO (5%)	-1.1	0.29×10^{-4}
TiO_2/ZnO (10%)	-1.0	0.25×10^{-4}

Photocatalytic activity of TiO_2 and TiO_2/ZnO films has been tested in the photoreduction of toxic Cr*(*VI*)* to non-toxic Cr*(*III*)* ions in acid water solutions in the presence of environmentally important substrate EDTA (Table 1). This process has been taken as a model of real wastewaters where oxidizing and reducing agents are present together for comparable studies of commercial samples and platinized TiO_2 powders[32]. The mechanism of photocatalytic Cr (VI) reduction in the presence of electron donors (EDTA, salicylic acid or other organic molecules) is well described herein[33]. Under irradiation in the presence of TiO_2/ZnO films, the changes in Cr*(*VI*)* concentration was followed by the decrease of absorption band intensity at 349 nm, simultaneously the absorption at 550 nm increased due to non-toxic Cr*(*III*)* formation (Fig.4.)

Efficiency of toxic Cr(VI) ions photoreduction grows in correlation with the flat-band potential shift to more negative values (from −0.51 V for TiO_2 to −1.1 V vs NHE for TiO_2/ZnO 1% samples). Doping of TiO_2 by 1-5% of Zn^{2+} ions leads to increase the reaction rate constant from 0,22 to 0,30 $\times10^4$ c^{-1}, however the grow of Zn^{2+}content from 1 to 10% causes to the diminishing of films photoactivity. Improvement of efficiency of TiO_2/ZnO samples with low Zn^{2+} content as compared to pure TiO_2 films can be explained by the formation of new acid centres on the surface of mixed oxides[1-3, 21] and increase of lifetime of photogenerated electron-hole pair (e^- and h^+) due to the appearance of new crystalline phase ZnO or $Zn_2Ti_2O_8$[6,7, 20-22]. Drop of catalytic efficiency for 10%ZnO/TiO_2 films can be connected with the low active $ZnTiO_3$ phase formation[7, 21].

3.3. Phase Composition and Electronic Structure of TiO_2/ZrO_2 Films

The adsorption-desorption isotherms of hexane on 773K calcined TiO_2 and ZrO_2/TiO_2 samples[15] demonstrated the type IV shape which indicated the presence of mesoporosity

in accordance with[27]. The specific surface areas (S_{BET}) and mean pore sizes of ZrO_2/TiO_2 films annealed at 773K are listed in Table 2. Uniform porosity with r= 8-10 nm typical for samples with low ZrO_2 content. Pure TiO_2 and 30% TiO_2/ZrO_2 films shows broader pore size distribution shifted to the larger pores with radius around 14 nm.

Table 2. Surface characteristics of TiO_2 and TiO_2/ZrO_2 mesoporous films calcined at 773K

Sample characteristics		
Sample	S_{BET}, m^2/g	Pore radii, nm
TiO_2 nonporous*	-	-
TiO_2	816	3.8; 6.1; 13.8
TiO_2/ZrO_2 (5% ZrO_2)	1007	8.2
TiO_2/ZrO_2 (10% ZrO_2)	557	3.8, 9.7
TiO_2/ZrO_2 (30% ZrO_2)	123	3.8; 14.2

*For film prepared without template, S_{BET} cannot be measured directly

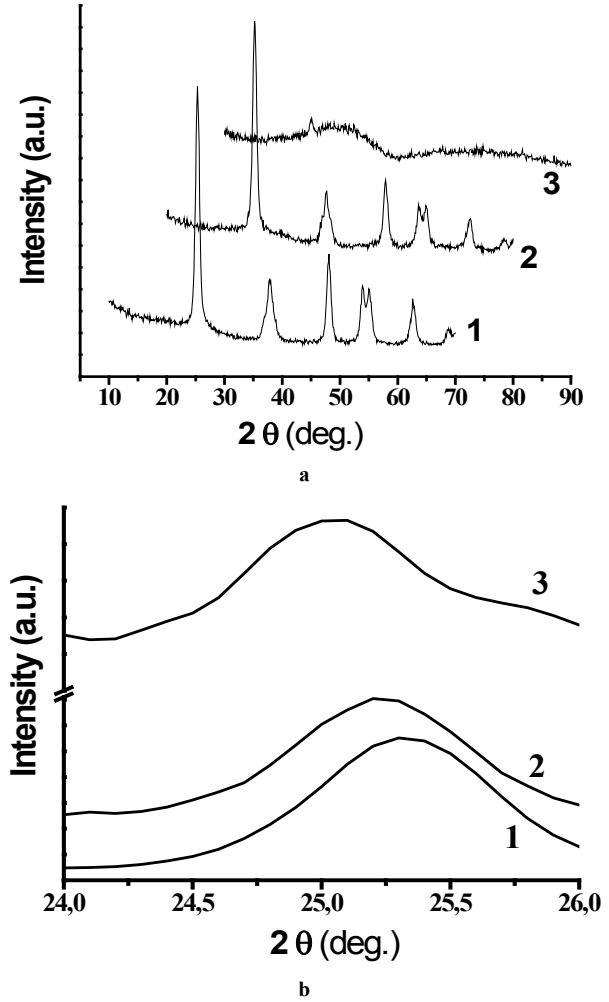

Figure 5. a). XRD patterns and b). XRD peaks of anatase crystal plane (101) of the powders after calcinations at 773K: TiO_2 (1) and TiO_2/ZrO_2 (2 – 10, 3 – 30 mol.% of ZrO_2)

Only anatase phase (JCPDS-ICDD, №21-1272) was identified in XRD patterns of TiO_2 and TiO_2/ZrO_2 powders prepared from the precursors. XRD measurements of TiO_2/ZrO_2 powders in the range of ZrO_2 concentrations 5-30 mol.% did not reveal any peaks, typical for crystalline zirconia phase. Whereas TiO_2 and TiO_2/ZrO_2 (5-10% ZrO_2) powders show high crystallinity (80-70%) with 9-11 nm anatase nanoparticles, TiO_2/ZrO_2 (30%) powder was amorphous after calcination at 673K. The Increase of the calcination temperature up to 773K led to the insignificant grows of crystallinity for TiO_2/ZrO_2 samples with low zirconium content.

Powder with 30 mol. % of ZrO_2 after treatment at 500℃ showed only weak reflex at 2θ = 25.4 characteristic for TiO_2 anatase on the amorphous matrix background.

These results indicate that in the TiO_2/ZrO_2 binary oxides, crystallization of titanium oxide is suppressed when Zr content increases due to the zirconia retarding effect on anatase crystallites' growth[34]. Detailed analysis of XRD spectra of the TiO_2/ZrO_2 powders proved the formation of solid solution $Ti_{1-x}Zr_xO_2$ with anatase structure as resulted from the anatase (101) crystal plane reflection shift into lower 2θ region (fig. 3b) due to the differences in the ionic radii of Zr^{4+} and Ti^{4+}. The increase of lattice parameters and cell volume of solid solutions $Ti_{1-x}Zr_xO_2$ as function of zirconium content (x) was observed[37, 38, 16].

The application of Raman spectroscopy considerably expands the possibilities of study of the material structure, the phase transformation peculiarities, the quantum size effect, compositional effects, the material evolution with sintering and treatment. The group-theoretical analysis gives the existence of 15 optical modes in the centre of Brillouin zone of anatase TiO_2: $\Gamma_{dis}=A_{1g}+A_{2u}+B_{1g}+B_{2u}+3E_g+2E_u$ Among these modes, A_{1g}, B_{1g} and $3E_g$ are Raman active, and modes A_{1u}, B_{1u}, $2E_u$ are infrared active.

Raman spectra of TiO_2 and TiO_2/ZrO_2 nanocrystals with different concentration of ZrO_2 heat treated at 773K were analyzed in[35]. The number and frequencies of the Raman bands for TiO_2 coincide with obtained in previous studies for anatase powder and single crystal[36]. The Raman bands at 148, 401, 522 and 648 cm^{-1} can be assigned as the E_g, B_{1g}, A_{1g} or B_{1g} and E_g modes of anatase phase, respectively. No other bands characteristic for other polymorphs were found. As ZrO_2 concentration increases, the bands became broader; some of them are shifted (148, 401 cm^{-1}). Raman spectrum for TiO_2/ZrO_2 (30%) sample changes dramatically: the intensity decreases while the width at half maximum of the bands increases, and some new bands appear (Fig. 6a).

The spectrum of sol-gel derived ZrO_2, which can be described as a mixture of amorphous zirconia and *t*-ZrO_2 is presented as reference.

Raman spectra of the TiO_2 and TiO_2/ZrO_2 5% films annealed at 773K (4 layers) are shown in the fig. 7. The Raman bands at 141, 396, 454, 520, 593 and 632cm^{-1} have been detected. In general, Raman spectra of the films are similar to the spectra of corresponding powders, but all bands broaden and shift towards higher or lower wavenumbers depending on the type of vibration. Formation of the crystalline structure for the TiO_2/ZrO_2 mesoporous films with zirconia concentration 10-30 mol.% was not registered, most probably due to their amorphous character that coincides well with our results of AFM and XRD mentioned above.

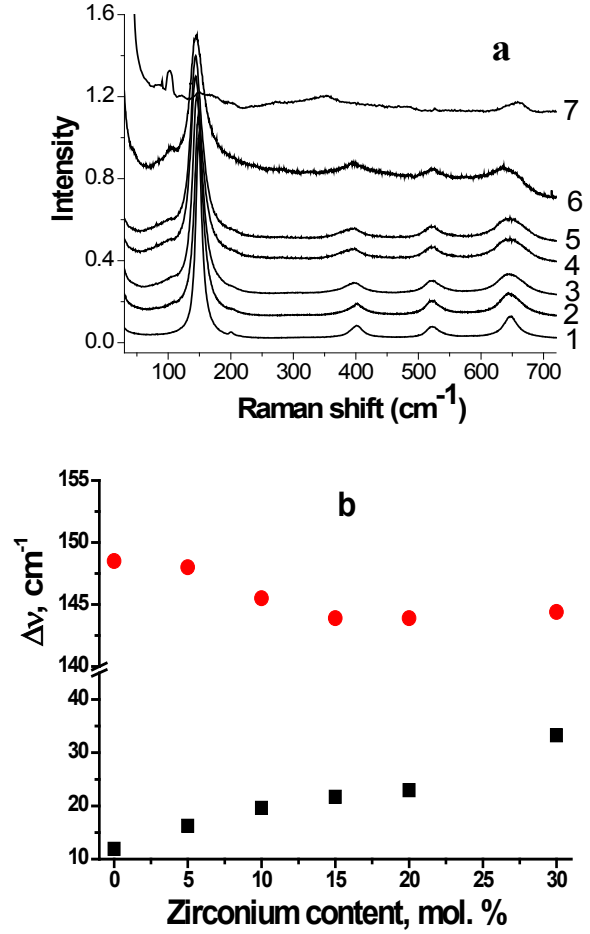

Figure 6. a - Raman spectra of TiO_2 (1), TiO_2/ZrO_2 (2 – 5%, 3 – 10%, 4 – 15%, 5 – 20% and 6 – 30% of Zr) and ZrO_2 (7) powders; b - Frequency (circles) and linewidth (squares) of E_g mode of TiO_2 as a function of Zr-concentration

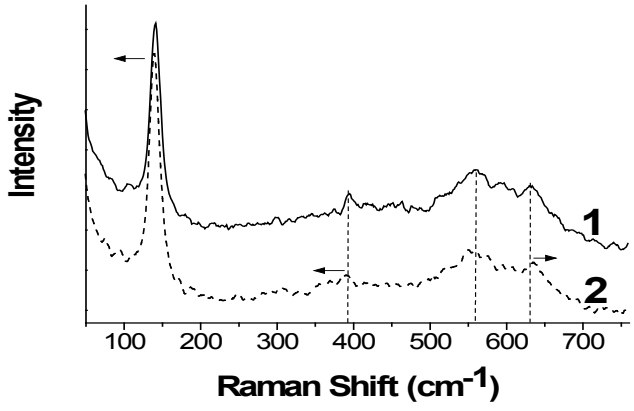

Figure 7. Raman spectra of the TiO_2 – 1) and TiO_2/ZrO_2 5% - 2) films annealed at 773K

Thus, we can conclude that the sol-gel method utilized in this study for the mesoporous TiO_2/ZrO_2 powders and films preparation with simultaneous hydrolysis of titanium and zirconium alkoxides in the presence of complexing agent – acetylaceton, ensures precursor components mixing at molecular scale with formations of numerous Ti – O – Zr bridges. This, in turn, leads to the new matrix formation – solid solution of zirconium in TiO_2 with anatase structure at certain Zr content range.

The electronic structure of nanosized zirconia-doped titanium dioxide films (5–30mol.% ZrO_2) has been investigated by means of XPS. The main contribution to the Ti*2p*-line of all samples has the component with the binding energy Ti*2p*3/2 = 458.5 eV. With increasing doping, the contribution of the component of E_B Ti*2p*3/2 = 458.9 eV grows. Within this range of energies, structurally nonequivalent TiO_2 phases are usually observed[29] The correlation between the relative contribution of the component with E_B Ti*2p*3/2 = 458.9 eV to Ti*2p*–spectra and the relative content of the doping element in the films (Table 3) can indicate the formation of the $ZrTiO_4$ phase[29] or the solid solution $Ti_{1-x}Zr_xO_2$[37, 38]

The components with E_B Zr*3d5*/2 = 181.6 eV and E_B Zr*3d5*/2 = 182.3 eV in Zr*3d*-spectra of ZrO_2 and TiO_2/ZrO_2 films can be correlated with nonequivalent zirconium atoms of the Ti-O-Zr bonds (phase 1 and phase 2 respectively)[29, 39]. The contribution of phase 1 (E_B = 181.6 eV) into Zr3d-spectrum diminishes with increase of dopant content, the contribution of the phase 2 (E_B = 182.3 eV) is maximal for the sample TiO_2/ZrO_2 (30 mol.%). A decrease in the contribution of the component with E_B $Zr3d_{5/2}$ = 181.6 eV can be caused by the absorption effects due to the localization of the phase 2 on the surface of microcrystallites of the phase 1. Taking into account the results of deconvolution of the Ti2p-spectra, the signal in the range of E_B $Zr3d_{5/2}$ = 181.6 eV can be related to the formation of a $ZrTiO_4$ phase[29] or $Ti_{1-x}Zr_xO_2$ (solid solution of Zr in TiO_2)[37] that is more probable, as XRD and Raman spectra analysis of corresponding powders after calcinations at 500°C showed the presence of only one crystalline phase – anatase with slightly distorted lattice parameters.

The results of spectra deconvolution into O1s-components for investigated samples are presented in the Table.3. The signals in the range of E_B O1s = 529.8–530 eV correspond to the O^{2-} -state of oxygen atoms in the oxide lattices of titanium and zirconium[29].

In the range of E_B O1s = 531.2–531.8 eV, contributions of oxygen of different OH-groups, which are surface active sites for the investigated samples are observed[29]. The maximum content of OH-groups is observed for the sample TiO_2/ZrO_2 (10 mol.%) (Table 3), probably indicating an increase of the quantity of the surface active sites on the surface unit. Thus, XPS investigation showed that formation of the photocatalytically active phase $Ti_{1-x}Zr_xO_2$ takes place when template assisted sol-gel method of synthesis of zirconium-doped TiO_2 mesoporous films is used for a dopant loading up to 10%. This phase is characterized by increased surface area at high crystallinity degree, with maximum quantity of hydroxyl groups for the sample TiO_2/ZrO_2 10mol.%. With increasing Zr concentration up to 30%, formation of amorphous ZrO_2 phase begins which is accompanied by a sharp decrease of surface area of the films and number of surface hydroxyl groups that will have pronounced influence on the photocatalytical activity of the films.

Table 3. Parameters of XPS spectra of TiO_2/ZrO_2 nanocomposites: binding energies E_B (eV) and integral intensities I (%) of the components for Ti*2p*-, Zr*3d*- and O*1s*- spectra

Binding energy, E_B		Content of ZrO_2 inTiO_2/ZrO_2 films, %				
		5	10	30	0	100
		Relative intensities of XPS peaks, %				
$Ti2p_{3/2}$	458.5 eV	96.3	89.9	74.1	100	-
	458.9 eV	3.7	10.1	25.9	0	-
$Zr3d_{5/2}$	181.6 eV	70.0	58.3	0	-	0
	182.30 eV	30.0	41.7	100	-	100
O1s	529.8–530 eV	94.2	87.7	89.5	92.4	93.1
	531.2–531.8 eV	5.8	12.3	10.5	7.6	6.9
Error ± 0.5						

3.4. Photoelectrochemical Characteristics and Photocatalytic Properties of TiO_2/ZrO_2 Films

Spectral dependences of photocurrent were measured for the TiO_2/ZrO_2 electrodes (TiO_2/ZrO_2 films were coated on Ti substrate) to obtain the value of the band gap energy.

For the tested TiO_2/ZrO_2 compositions, linear dependence in $(\eta \cdot h\nu)^{1/2} = f(h\nu)$ coordinates was not obtained due to some reasons such as: photocurrent in the long-wave spectral region caused by defects in the anatase structure and/or low intensity of photocurrent corresponded to indirect transition in thin films due to low absorption coefficient.

The obtained experimental data fit better to a direct transition[40]. Band gap (E_g) values were calculated by extrapolation of straight line of these dependences to the abscissa (Table 4). With growing of zirconium content, the increase of band gap values from 3.17 for TiO_2 to 3.45 eV for 50%ZrO_2/TiO_2 was observed that can be attributed to quantum-size effect[41]. This result indicates that titania doping with zirconum ions inhibits crystallite growing[2, 34].

Table 4. Photoelectrochemical characteristics and rate constants for Cr(VI) to Cr(III) photoreduction over mesoporous TiO_2/ZrO_2 films

Catalyst	E_g, eV	E_{fb},[V, NHE]	k, min^{-1}
TiO_2 (non-porous)	3.16	-0.51	$1.3 \cdot 10^{-2}$
TiO_2	3.17	-0.51	$1.9 \cdot 10^{-2}$
TiO_2/ZrO_2 (5% Zr)	3.26	-0.52	$2.3 \cdot 10^{-2}$
TiO_2/ZrO_2 (10% Zr)	3.29	-0.54	$2.0\ 10^{-2}$
TiO_2/ZrO_2 (30% Zr)	3.33	-0.55	$1.5 \cdot 10^{-2}$
TiO_2/ZrO_2 (50% Zr)	3.45	-0.52	$1.1 \cdot 10^{-2}$

The position of the flatband potential (E_{fb}) of the catalysts was determined by the direct electrochemical measurements of photocurrent as a function of applied potential in aqueous 0.5 NaCl. Flatband potentials were estimated from i_{ph} changes measured at the photocurrency maximum for TiO_2 and TiO_2/ZrO_2 films coated on the titanium substrate in aqueous 0.5M NaCl plotted against applied potential by extrapolation straight line of these dependences to the abscissa. Flatband potential values for the samples with different zirconium content differ insignificantly and are comparable with the value of -(0,47-0,49) V obtained at pH ≈7 for nitrogen-doped titanium dioxide[42] and U_{fb}= -0,58 V measured for anatase single crystal[43, 44].

Photocatalytic activity of mesoporous TiO_2 and TiO_2/ZrO_2 (5-30%) films, in comparison with films prepared without template, increases in accordance with increasing specific surface area of the samples. The conversion of $Cr_2O_7^{2-}$, calculated for mesoporous TiO_2 films, was 4 times higher, than that observed for nonporous samples and 10 times higher, than it was reported in[45] for the equal amount of TiO_2, supported on hollow glass microbeads during the same time of irradiation.

The enhanced activity was observed for TiO_2/ZrO_2 films with low concentration of zirconium that possessed the high surface area and composed from nanoparticles with mean size 3-4 nm. Zr doping retards not only anatase to rutile transformation, but also inhibits the crystalline growth[1-3, 34]. It can be seen that in general there is the increase of E_g with the anodic shift of the upper edge of the valence band positions as the Zr concentration increases. Processes of EDTA oxidation accelerate, improving charge separation, and Cr (IV) reduction proceeds faster due to synergism between the oxidation and reduction reactions. Further increasing of Zr content leads to low crystallinity of 30%ZrO_2/TiO_2 and amorphous structure of 50%ZrO_2/TiO_2 samples. This effect explains the drop of activity of these samples.

3.5. Phase Composition and Electronic Structure of $TiO_2/ZrO_2/SiO_2$ Films

Ternary $TiO_2/ZrO_2/SiO_2$ films were synthesized via sol-gel method without template addition to obtain photoactive mechanically strength coatings with high thermal, chemical and radiation stability. As was reported previously[24] prepared transparent nanosized ternary films had good optical quality (refractive index 1.82), remained stable and retained the high photocatalytic activity after β-irradiation as well as contact with aggressive chemical environment.

XRD analysis of ternary systems did not give clear information about crystalline structure of the composites. This is more likely due to the insufficient resolution of XRD method used for investigation of the nanosized systems than due to the formation of amorphous oxide network. In the XRD spectra of pure TiO_2 and ZrO_2 films deposited onto glass substrates and heat treated at 600°C can be distinguished reflections corresponding to the TiO_2 anatase and tetragonal ZrO_2 phases. As it was discussed previously common crystallization in the binary or ternary systems during oxide network formation causes inhibitive influence on the growth and agglomeration of the individual phases of the components, partly even due to the chemical interaction between components with formation of Ti-O-Si, Ti-O-Zr and Si-O-Zr bonds. Vogel et al[12] also reported formation of tiny crystallites of TiO_2 after calcination even at 623K. These titanium dioxide crystallites embedded into amorphous

oxide network were "amorphous for XRD" and detected by electron diffraction and bright field TEM.

Diffraction patterns of $TiO_2/ZrO_2/SiO_2$ powders prepared via gelation of the films precursors, their drying in air with following heat treatment at 873K, 973K and 1073K presented on Fig. 8. XRD analysis evidenced simultaneous crystallization of two crystalline phases – anatase and srilankite Ti_2ZrO_6[46-48].

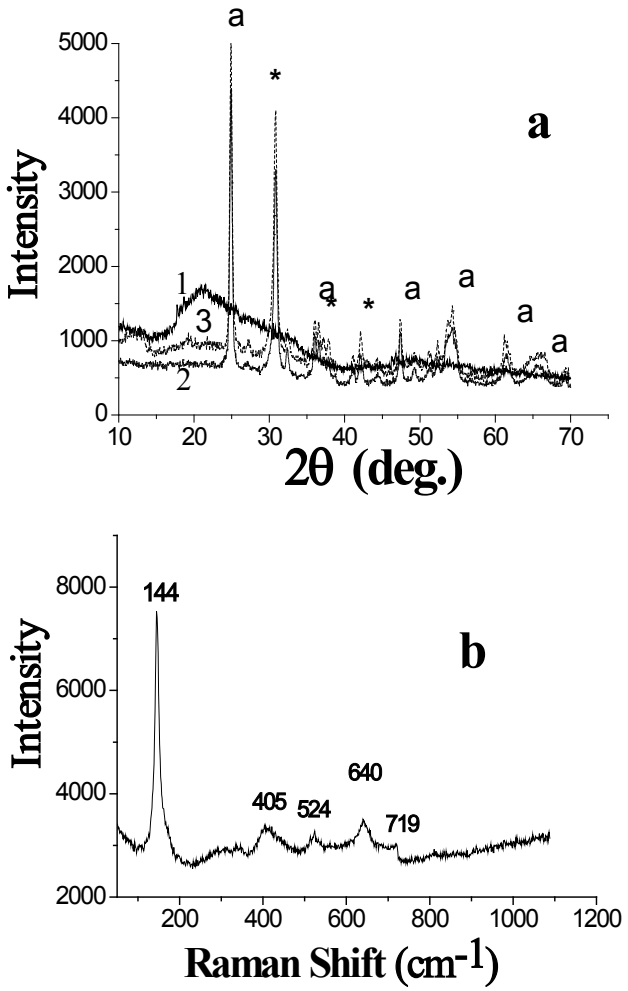

Figure 8. (a) X-ray diffraction patterns of $TiO_2/ZrO_2/SiO_2$ powders calcined at: 873K -1; 973K - 2; 1073K – 3; a – anatase, * - srilankite; (b) Raman spectra of $TiO_2/ZrO_2/SiO_2$ powder calcined at 1073K

The Raman spectrum of $TiO_2/ZrO_2/SiO_2$ powder (Fig.8, b) thermal treated at 800℃ depicts a set of reflexes related to anatase (lines at 146, 400, 525, 640 $см^{-1}$)[49, 50] and only one weaker reflex at 719$см^{-1}$, corresponding to ZrO_2[51].

Formation of chemical bonds between components in binary and ternary oxide mixtures was investigated using XPS method. For this purpose detailed spectra of binary and ternary sol-gel films and pure oxides were investigated and compared[23].

In oxygen O 1s and silicon Si 2p regions (Fig.9, a, b) one can see that the positions of O 1s and Si 2p peaks for Si-O bonds are negatively shifted relative to single SiO_2 in sample 1 and this shift depends on titanium and zirconium content in the mixed oxides.

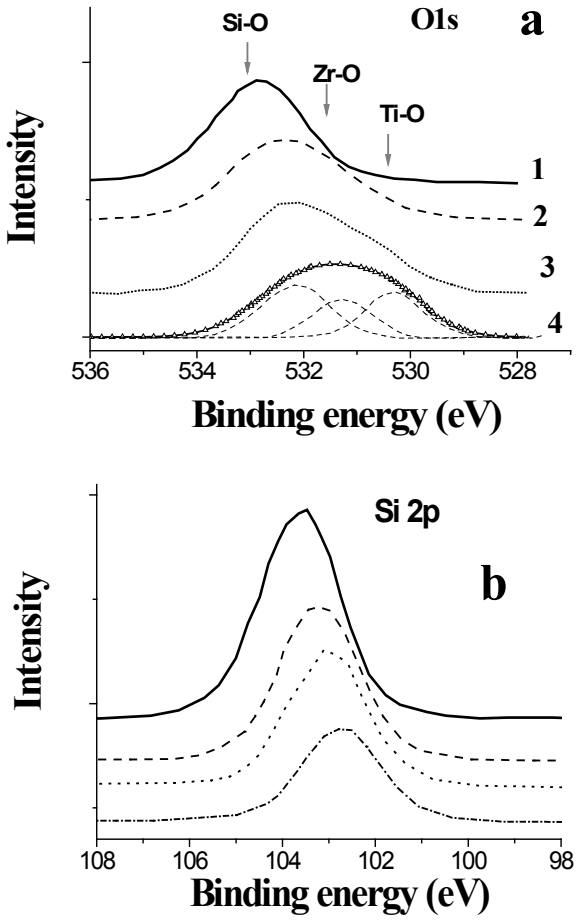

Figure 9. Detailed XPS (a) Si 2p region spectra and (b) O1s region spectra for sol-gel prepared pure SiO_2- 1 and mixed oxide films TiO_2/SiO_2 (30:70) – 2, $TiO_2/ZrO_2/SiO_2$ (21:9:70) – 3 and fitted into three peaks corresponding to the appropriate oxygen bonds $TiO_2/ZrO_2/SiO_2$ (49:21:30) – 4

In sample 1 oxygen O 1s and silicon Si 2p peaks positions (532.9 eV and 103.44 eV respectively) coincide with known[52] peak positions in SiO_2: O 1s peak - 532.89 eV and Si 2p peak - 103.6 eV. The shift of Si 2p peak is 0.51 eV in sample 2 and 1.03 eV in sample 4 then Ti atomic concentration changes from 0% to 20% and 36%, respectively. Such peak position shift suggests its uniform dependence on the Ti concentration. Ti $2p_{3/2}$ and Zr $3d_{5/2}$ peak positions (Fig. 10) for mixed oxides are shifted towards higher binding energies (positive shift) comparing to the peak position in sample of sol-gel prepared pure TiO_2 or ZrO_2 film.

Similar shift behaviors can be noticed for Si 2p – Ti 2p and Si 2p – Zr 3d peaks, therefore these shifts can be attributed to the formation of binary and ternary oxides with Si – O – Ti, Si – O – Zr, Ti – O – Zr, Si – O – Ti – O – Zr bonds.

Described above peaks shifts are in good agreement with the red shift of optical absorption for single and mixed oxides and E_g reduction from 8.9 eV for SiO_2 to 3.68 eV for $TiO_2/ZrO_2/SiO_2$ (49:21:30) film. It can be also mentioned that Si 2p and O 1s peaks position shift dependence correlates well with the photocatalytic activity of ternary $TiO_2/ZrO_2/SiO_2$ films in the process of Cr(VI) ions

photoreduction to Cr(III) state (Table 5).

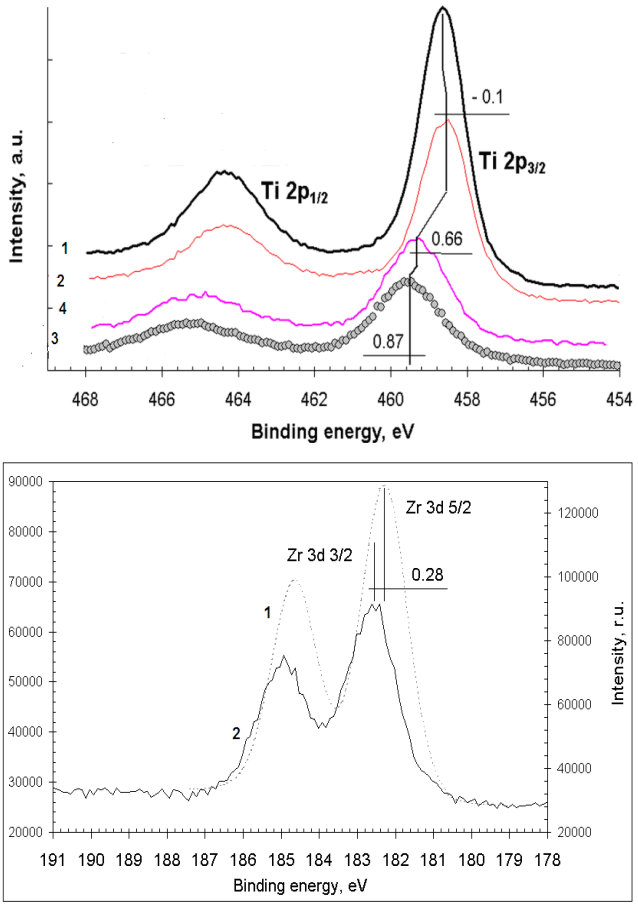

Figure 10. XPS (a) Ti 2p spectra for sol-gel prepared TiO_2- 1 and mixed oxide films TiO_2/ZrO_2 (70:30) – 2; TiO_2/SiO_2 (30:70) – 3, $TiO_2/ZrO_2/SiO_2$ (21:9:70) – 4; (b) Zr3d region spectra for pure ZrO_2 – 1 and TiO_2/ZrO_2 (70:30) – 2

Table 5. Rate constants for Cr(VI) to Cr(III) photoreduction over binary and ternary mixed oxide sol-gel films

Catalyst	Eg, eV	k, min^{-1}
SiO_2/ZrO_2 (70/30)	5.72	$0.50 \cdot 10^{-2}$
SiO_2/TiO_2 (70/30)	3.75	$0.51 \cdot 10^{-2}$
TiO_2/ZrO_2 (70/30)	3.61	$0.55 \cdot 10^{-2}$
$TiO_2/ZrO_2/SiO_2$ (21/9/70)	4.04	$0.60 \cdot 10^{-2}$

4. Conclusions

Sol-gel synthesis of nanostructured mixed oxide films (mesoporous TiO_2/ZnO and TiO_2/ZrO_2, nonporous $SiO_2/TiO_2/ZrO_2$) using metal alkoxides as precursors and acetylacetone as a complexing agent assures extensive bridging of components through the oxygen, which has pronounced influence on phase composition, electronic structure, photoelectrochemical characteristics and photocatalytic activity of obtained coatings.

In the case of TiO_2/ZnO nanocomposites, the crystallinity of the TiO_2/ZnO films slightly increased with Zn content and $ZnTiO_3$ perowskite phase is formed. The films with low Zn content (1-5%) showed superhydrophilicity. Direct photoelectrochemical investigation of the mesoporous TiO_2/ZnO films showed the cathodic shift of the flat band potential position and the increase of the photocurrent quantum yield in comparison with unmodified TiO_2 electrodes that coincided with the increase of their activity in the process of Cr(VI) photoreduction.

Zirconium incorporation into TiO_2 lattice with formation of $Ti_{1-x}Zr_xO_2$ solid solution containing anatase structure leads to increase of E_g with the anodic shift of the upper edge of the valence band position accelerating photocalytic processes due to the improvement of charge separation. The maximum content of OH-groups is observed for the sample TiO_2/ZrO_2 (10 mol.% ZrO_2) indicating an increase of the quantity of the surface active sites.

Under experimental conditions of sol-gel procedure of ternary systems formation, two crystalline phases are formed anatase and srilankite (Ti_2ZrO_6). Analysis of the XPS spectra showed the formation of Si – O – Ti, Si – O – Zr, Ti – O – Zr, Si – O – Ti – O – Zr bonds. Oxygen and silicon peak positions evolution detected by XPS correlate with E_g reduction of analyzed mixed oxides that resulted in the substantial increase of photocatalytic activity in the process of Cr (VI) ions photoreduction.

ACKNOWLEDGEMENTS

The authors gratefully acknowledge M. Andrulevičius in the assistance of XPS measurements $SiO_2/TiO_2/ZrO_2$ and Prof. S. Tamulevičius for fruitful discussion.

REFERENCES

[1] M. E. Zorn, D. T. Tompkins, W. A., Zeltner, and M. A. Anderson, 2000, Catalytic and Photocatalytic Oxidation of Ethylene on Titania-Based Thin-Films., Environ. Sci. Tech., 34(24), 5206-5210.

[2] M.E. Manriquez, T. Lopez, R. Gomez, and J. Navarrete, 2004, Preparation of TiO_2-ZrO_2 mixed oxides with controlled acid-basic properties., J. Mol. Catal. A-Chem., 220, 229-237.

[3] X. Fu, L.A. Clark, Q. Yang, and M.A. Anderson, 1996, Enhanced Photocatalytic Performance of Titania-Based Binary Metal Oxides: TiO_2/SiO_2 and TiO_2/ZrO_2., Environ. Sci. Tech., 30(2), 647–653.

[4] L. Valdez – Castro J. Méndez – Vivar, and R. Mendoza – Serna, 2001, Porous SiO_2–TiO_2–ZrO_2 Obtained from Polymeric Systems Prepared by the Sol–Gel Process, J. Porous Mat., 8, 303 – 309.

[5] T. Ivanova, A. Harizanova, T. Koutzarova, and B. Vertruyen, 2011, Preparation and characterization of ZnO–TiO_2 films obtained by sol-gel method., J. Non-Cryst. Solids, 357, 2840–2845.

[6] G. Marci, V. Augugliano, and M.J. López-Muñoz, 2001, Preparation, characterization and photocatalytic activity of

polycrystalline ZnO/TiO_2 systems., Surface and bulk characterization, J. Phys. Chem. B, 105, 1026-1040.

[7] S. Liao, Y. Donggen, D. Yu, Y. Su, and G. Yuan, 2004, Preparation and characterisation of ZnO/TiO_2, $SO_4^{2-}/ZnO/TiO_2$ photocatalyst and their photocatalysis., J. Photochem. Photobiol. A, 168(1-2), 7–13.

[8] A. Sclafani, L. Palmisano, and M. Schiavelo, 1990, Influence of the preparation methods of titanium dioxide on the photocatalytic degradation of phenol in aqueous dispersion., J. Phys. Chem., 94(2), 829–832.

[9] T. Lopez, R. Gomez, E. Sanchez, F. Tzompantzi, and L. Vera, 2001, Photocatalytic Activity in the 2,4-Dinitroaniline Decomposition Over TiO_2 Sol-Gel Derived Catalysts., J. Sol-Gel Sci. & Techn., 22(1-2), 99-107.

[10] M. Gärtner, V. Dremov, P. Müller, and H. Kisch, 2005, Bandgap widening of titania through semiconductor support interactions., ChemPhysChem, 6(4), 714-722.

[11] N.F. Uvarov and V.V. Boldyrev, 2001, Size effects in the chemistry of heterogeneous systems., Usp. Khim., 70(4), 307-329.

[12] A.A. Gribb and J. F. Banfield, 1997, Particle size effects on transformation kinetics and phase stability in nanocrystalline TiO_2., Amer. Mineral, 82 (7-8), pp. 717-728.

[13] S.J. Smith, R. Stevens, S. Liu, G. Li, A. Navrotsky, J. Boerio-Goates, and B. F. Woodfield, 2009, Heat capacities and thermodynamic functions of TiO_2 anatase and rutile: Analysis of phase stability, Amer. Mineral., 94(2-3), 236-243.

[14] P. Yang, D. Zhao, D.I. Margolese et al., 1998, Generalized syntheses of large-pore mesoporous metal oxides with semicrystalline frameworks, Nature (London), 396, 152–155.

[15] R. Vogel, P. Meredith, I. Kartini, M. Harvey, J. Riches, A. Bishop, N. Heckenberg, M. Trau, and H. Rubensztein-Dunlop, 2003, Mesostructured Dye-Doped Titanium Dioxide for Micro-Optoelectronic Applications., ChemPhysChem, 4, 595-603.

[16] Yu. Gnatyuk, N. Smirnova, A. Eremenko, and V. Ilyin, 2005, Design and Photocatalytic activity of mesoporous TiO_2/ZrO_2 thin films., Ads. Sci. & Techn., 23, 497-503.

[17] I. Petrik, O. Kelyp, V. Vorobets, N. Smirnova, O.Frolova, O. Oranska, G. Kolbasov, and A. Eremenko, 2011, Synthesis, optical, photo- and electrocatalytic properties of nanosized TiO_2 modified with transition metal ions., Chem., Phys. & Techn. Surf., 2(4), 436–442.

[18] Yu. I. Gnatyuk, V. I. Yatskiv, N. P. Smirnova, V. M. Granchak, and A. M. Eremenko, 2005, Photocatalytic properties of mesoporous TiO_2/ZrO_2 films in gas-phase oxidation of alcohols., Theoret. Experim. Chem., 41(6), 371-376.

[19] Yu. Gnatyuk, N. Smirnova, O. Korduban, and A. Eremenko, 2010, Effect of zirconium incorporation on the stabilization of TiO_2 mesoporous structure., Surf. Interface Anal., 42, 1276 – 1280.

[20] E. Manujlov, Yu. Gnatyuk, N. Smirnova, A.Eremenko, V. Vorobets, G. Kolbasov, A. Guobiené, and S. Tamulevicius, Mesoporous TiO_2 and TiO_2/ZnO/Ag films: sol-gel synthesis, photoelectrochemical and photocatalytic properties., P. Innocenzi, Yu. Zub, V. Kessler Eds. Springer, 2008.

[21] T. Ptashko, N. Smirnova, A. Eremenko, E. Oranska, and W. Huang, 2007, Synthesis and photocatalytic properties of mesoporous TiO_2/ZnO films with improved hydrophylisity., Ads. Sci. & Techn, 25, 35-43.

[22] N. Smirnova, V. Vorobets, O. Linnik, E. Manuilov, and G. Kolbasov, 2010, Photoelectrochemical and photocatalytic properties of mesoporous TiO_2 films modified with silver and gold nanoparticles., Surf. Interface Anal., 42, 1205 – 1208.

[23] M. Andrulevičius, S. Tamulevičius, Yu. Gnatyuk, N. Vityuk, N. Smirnova, and A. Eremenko, 2008, XPS investigation of $TiO_2/ZrO_2/SiO_2$ films modified with Ag/Au nanoparticles., J. Mat. Sci. (MEDŽIAGOTYRA), 149(1), 8 – 14.

[24] N.V. Vityuk, A.M. Eremenko, N.P.Smirnova, P.P. Gorbik, T. Busko, M.P. Kulish, O.P. Dmitrenko, V.V. Shlapatska, and V.A. Khizhny, 2007, Effect of irradiation on structural and photocatalytic properties of nanosized $TiO_2/ZrO_2/SiO_2$ composites., Phys. Chem. Solid State, 8(4), 776 – 781.

[25] O. Linnik and H. Kisch, 2006, On the mechanism of nitrogen photofixation at nanostructured iron titanate films., Photochem. Photobio. Sci., 5, 938-942.

[26] N. Smirnova, Yu. Gnatyuk, A. Eremenko, G. Kolbasov, V. Vorobetz, I. Kolbasova, and O. linyucheva, 2006, Photoelectrochemical characterization and photocatalytic properties of mesoporous TiO_2/ZrO_2 films., Intern. J. Photoenergy, 8, 1-6.

[27] S.I. Gregg and K.S.W. Sing, Adsorption, Surface Area and Porosity" Academic Press, London, 1982.

[28] C.C. Hyun, M.J. Young, and B.K. Seung, Size effects in the Raman spectra of TiO_2 nanoparticles., Vibrational Spectr., 37, 33–38, 2005.

[29] C.D.Wagner, J. F.Moulder, L. E. Davis, W. M. Riggs, Handbook of X-ray Photoelectron Spectroscopy, Perking - Elmer Corp.: New York, AQ4 1979.

[30] Tanabe K., Catalysis: Science and Technology. Anderson JR, Boudart M Eds. Springer, New York, 1981.

[31] V. Vorobets, E. Manujlov, N. Smirnova et al., 2008, Electro- and photocatalytic properties of electrodes based on mesoporous TiO_2-ZnO-Ag films., Chem., Phys. & Techn. of Surf., 14, 382-390.

[32] U. Siemon, D. Bahnemann, J. J. Testa, D. Rodríguez, M. I. Litter, and N. Bruno, 2002, Heterogeneous photocatalytic reactions comparing TiO_2 and Pt/TiO_2., J. Photochem. Photobio. A, 148(1–3), 247–255.

[33] G. Colon, M. C. Hidalgo, and J. A. Navio, 2001, Photocatalytic Deactivation of Commercial TiO_2 Samples During Simultaneous Photoreduction of Cr(VI) and Photooxidation of Salicylic Acid., J. Photochem. Photobio., A , 138(1) 79-85.

[34] J. Kim, K.C. Song, S. Foncillas, and S.E. Pratsinis, 2001, Dopants for synthesis of stable bimodal porous titania., J .Eur. Ceram. Soc., 21, 2863-2872.

[35] A. Naumenko, Iu. Gnatiuk, N. Smirnova, and A. Eremenko, 2012, Characterization of sol–gel derived TiO_2/ZrO_2 films and powders by Raman spectroscopy., Thin Solid Films, 520(14), pp. 4541–4546.

[36] T. Ohsada, F. Izumi, and Y. Fujiki, 1978, Raman spectrum of anatase., TiO_2, J. Raman Spectrosc., 7(6), 321-324.

[37] J.C. Yu, J. Lin, and R.M.W. Kwok, 1998, $Ti_{1-x}Zr_xO_2$ solid solutions for the photocatalytic degradation of acetone in air., J. Phys. Chem. *B*, 102, 5094 – 5098.

[38] M. Durr, S. Roselli, A. Yasuda, and G. Nelles, 2006, Band-gap engineering of metal oxides for dye-sensitized solar cells, J. Phys. Chem. *B*, 110(43), 21899- 21902.

[39] Nefedov V.I., Roentgenoelectronic spectroscopy of chemical compounds, Chemistry, Moskow, 1984.

[40] Yu. Ja. Gurevitch and Yu. V. Pleskov, Photoelectrochemistry of Semiconductors, Nauka, Moscow, 1983.

[41] A. L. Linsebigler, G. Lu, and J. T. Yates, 1995, Photocatalysis on TiOn Surfaces: Principles, Mechanisms, and Selected Results., Chem. Rev., 95, 735-758,.

[42] S. Sakthivel and H. Kish, 2003, Photocatalytic and photoelectrochemical properties of nitrogen-doped titanium dioxide., ChemPhysChem, 4. 487-490.

[43] M. Gratzel, S. E. Gilbert, C. Klemenz, and H. J.Scheel, 1996, Electrochemical and photoelectrochemical investigations of single-crystal anatase., J. Amer. Chem. Soc., 118, 716-6723.

[44] Ye. V. Kuzminskii and G. Ya. Kolbasov, 1999, Electrochemical systems for converting solar energy., Solar Ener. Mat. Solar C., 5, 93-115.

[45] Chen, Shi-Fu, and Xue-Li Cheng, 1999, Photocatalytic Reduction of Dichromate by Titanium Dioxide Supported on Hollow Glass Microbeads., Chin. J. Chem., 17(4), 419-24.

[46] U. Diebold, 2003, The surface science of titanium dioxide., Surf. Sci. Reports, 48, 53 – 229.

[47] J.-Chr. Buhl and A. Willgallis, 1989, Hydrothermal synthesis of $(Zr_{0.33}\ Ti_{0.67})\ O_2$-srilankite in the system ZrO_2-TiO_2-H_2O-MF; (M = Na, K)., Cryst. Res. Techn., 24, 263 – 268.

[48] U. Troitzsch, A.G. Christy, and D.J. Ellis, 2005, The crystal structure of disordered $(Zr,Ti)O_2$ solid solution including srilankite: evolution towards tetragonal ZrO_2 with increasing Zr., J. Phys. Chem. Minerals, 32, 504 – 514.

[49] W.F.Zhang, Y.L.He, M.S.Zhang, Z.Yin and Q.Chen, 2000, Raman scattering study on anatase TiO_2 nanocrystals., J. Phys. D: Appl. Phys, 33, 912 – 916.

[50] F.M.Liu, B.Ren, J.H.Wu, J.W.Yan, X.F.Xue, B.W.Mao, and Z.Q.Tian, 2003, Enhanced Raman scattering from silicon nanoparticle substrates., Chem. Phys. Lett., *382*, 502-507.

[51] S.N.Tkachev, M.H.Manghnani, A.Niilisk, J.Aarik, and H.Mändar, 2005, Raman and Brillouin scattering spectroscopy studies of atomic layer-deposited ZrO_2 and HfO_2 thin films., Spectrochim. Acta A, 61, 2434-2438.

[52] C. D. Wagner, A. V. Naumkin, A. Kraut-Vass, J. W. Allison, C. J. Powell, and J.R. Rumble Jr. *NIST Standard Reference Database* 20, Version 3.4